Identification of Self-Buffer Layer on GaN/glass Films Grown by Reactive Sputtering

R. S. de Oliveira[a], H. A. Folli[a], I. M. Horta[a], B. S. Damasceno[a], J. H. C. Augstrose[a], W. Miyakawa[a],

A. L. J. Pereira[a], M. Massi[b] (iD) *, A. S. da Silva Sobrinho[a]* (iD) *, D. M. G. Leite[a]** (iD)

*[a]Instituto Tecnológico de Aeronáutica (ITA), Laboratório de Plasmas e Processos (LPP),
São José dos Campos, SP, Brasil.
[b]Universidade Presbiteriana Mackenzie, Escola de Engenharia, São Paulo, SP, Brasil.*

This work reports on the properties of GaN films grown by reactive magnetron sputtering onto glass substrate kept at relatively low temperature (400°C), using different RF power applied to the Ga target. Their structural, morphological, vibrational and optical properties were characterized by X-ray diffraction, atomic force and scanning electron microscopies, Raman spectroscopy and UV-vis spectrophotometry. The films have wurtzite phase with strong preferential orientation in the *c*-axis direction. Moreover, two clear contributions to the (0002) diffraction peak could be found, indicating the presence of two different morphologies, which were discussed in terms of the formation of an intermediate layer between the substrate and a dominating columnar-like microstructured film.

Keywords: *GaN, reactive sputtering, buffer layer, glass substrate.*

1. Introduction

GaN is an attractive semiconductor due to its wide direct band-gap (3.4 eV), high electronic mobility, and high melting point temperature (2,500°C)[1]. These properties have resulted in the development of blue and UV LEDs and lasers, as well as improvements in many other applications such as high electronic mobility transistors - HEMTs[2,3]. Furthermore, the GaN piezoelectric properties have enabled its use in high frequency (above 5 GHz) filters and sensors, which has allowed it to surpass other materials such as ZnO and AlN in some cases[4,5].

The reactive sputtering technique is a cost-effective low-temperature method for GaN film growth, with relative high deposition rates, and suitable for a wide range of different substrate sizes[6,7]. Temperatures below 600°C strongly favor the growth in the <0002> direction[8]. This is extremely advantageous, as the production of high-quality, electronic-grade GaN typically relies on sapphire (Al_2O_3) or silicon carbide (SiC) substrates, which are typically small and expensive. Therefore, the growth of GaN on glass substrates[9] is an appealing low-cost option, compatible with existing technologies. Additionally, the reactive sputtering technique has recently been used to produce GaN and AlN epitaxial films[10,11], while it was previously known to yield mostly amorphous or polycrystalline films.

The piezoelectric character of the GaN, even with a micro- or nanocrystalline structure, makes it interesting to applications such as surface acoustic waves (SAW) filters and sensors, and other high frequency devices[12-14]. To optimize and understand the physical properties of GaN films grown by sputtering with various deposition setups[15] onto different types of substrates, practical studies are in high demand.

In this context, a GaN-dedicated sputtering system was recently assembled in our laboratory. The first results were published in 2021[16], focusing on the influence of the RF power applied to the Ga target on the properties of the films grown onto Si (100) substrates. However, GaN/glass films grown simultaneously during that set of experiments exhibited significantly different results from those obtained for the GaN/Si films, showing no significant trend associated with the RF power. Therefore, this work presents the main findings of the GaN/glass samples, which rely on XRD data indicating the formation of an intermediate layer between the substrate and the main film morphology, which the authors have named self-buffer. This intermediate layer is rarely explored in reports on GaN/glass films grown by reactive sputtering. The samples were also characterized using atomic force and scanning electron microscopies, Raman spectroscopy, and spectrophotometry in the UV-Vis.

2. Experimental Details

The GaN films were grown on a recently assembled GaN-dedicated RF-magnetron sputtering setup described elsewhere[16]. The GaN/glass samples treated in this work were simultaneously grown with the GaN/Si samples, whose results were already published[16]. The main growth procedure details are in the following paragraph.

Standard boron silicate glass pieces of 12 x 12 mm were cleaned according to the standard RCA procedure, and then attached to stainless steel substrate holder disk placed 90 mm above the target surface. Before deposition, the substrates were heated up to 450°C for 30 minutes to outgas their surfaces up to 3×10^{-4} Pa residual pressure. Substrates were then left to cool down to the deposition

temperature of 400°C, as monitored by an optical pyrometer, and the deposition process started 30 minutes later, assuring uniform and stabilized substrate temperature. During the deposition, the substrates rotated at 6 rpm, to guarantee a homogeneous temperature (< 1°C variation along the substrate holder). The N_2:Ar flow rate of 14:7 sccm, the working pressure of 0.40 Pa and the 120 min deposition time are parameters chosen from preliminary tests. The samples were grown using RF powers of 30, 45, 60, 75 and 90 W. To avoid artifacts (false behaviors influenced by "memory effect"), all samples were grown out of the logical crescent sequence. The reproducibility was also confirmed by repeating the experiments with same deposition parameters.

The GaN thin films morphologies were examined by field emission gun scanning electron microscopy (FEG-SEM), using a Tescan microscope, model MIRA 3 and by atomic force microscopy (AFM), using a Shimadzu scanning probe microscope, model SPM 9500J3. The samples were also analyzed by X-ray diffractometry, using a PANalytical Empyrean, with Cu target (K_α radiation 1.5418 Å), under 40 kV and 40 mA, in Theta-2Theta geometry at 0.05°/s scan speed. Raman analyses were performed at room temperature, using a Horiba LabRAM HR Evolution Raman microscope, with a 532 nm laser and a 100x objective. Care was taken to avoid surface recrystallization due to a possible localized heat from the laser absorption. The UV-VIS-NIR T% spectra were taken using an Evolution 220 UV Visible spectrophotometer by Thermo Fisher Scientific. The T% spectra were then subjected to a fitting routine[17] based on the Joint Density of States model with parabolic band approximation[18,19] for the absorption edge and Wemple and DiDomenico model[20] for refractive index dispersion, from where the band-gap energy, the static refractive index and the film thickness were determined, the latter being confirmed by a mechanical profilometer KLA Tencor P7.

3. Results and Discussion

Figure 1 shows the transmittance spectra in the UV-Vis range of the produced GaN/glass samples, comparatively with the glass substrate without film deposition. The regularity of the interference fringes in the transparent region (above 450 nm) and the steep decrease of T% in the band-gap region are well known signatures of dense and homogeneous films with good optical quality[21,22]. Figure 2 shows the determined values of the static refractive index and the band-gap energy versus the applied RF power, showing slight deviations from the expected values of 2.24 and 3.4 eV, respectively[22]. Both the refractive index and the band-gap energy values for the 30 W samples have significant lack of precision and accuracy due to its very low thickness (~100 nm) combined with the glass substrate transmittance cut-off at 300 nm. From 45 to 90 W, which shows reliable values, it is not possible to identify any clear dependency of the refractive index and band-gap on the RF power applied to the Ga target. On the other hand, the thickness of the films shows a strong dependency of the RF power, as expected, which can be observed in Figure 3. In our previous work, regarding the GaN/Si samples[16], the film thickness dependence on the RF power was demonstrated and the deposition rate had been 0.6 nm/min at 30 W (about a tenth of that at 90 W), resulting in a thinner film with an incomplete interference fringe in the examined T% spectra region.
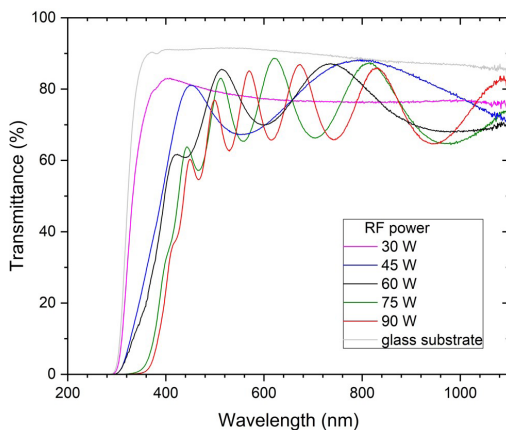
Figure 1. Transmittance spectra in the UV-Vis-NIR range of the produced GaN/glass films.
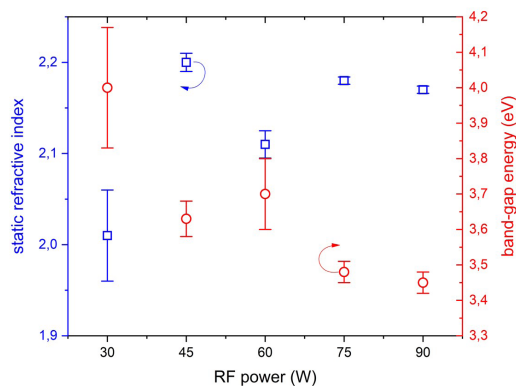
Figure 2. Static refractive index and band-gap energy as a function of the RF power.
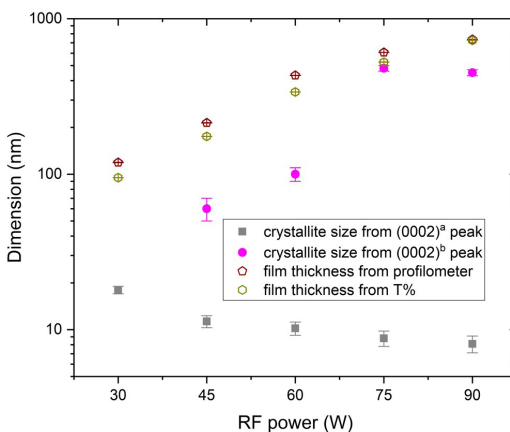
Figure 3. Crystallite size and film thickness as a function of the RF power.

Figure 4 shows the Raman spectra from the GaN/glass samples. Two well-known wurtzite-GaN phonon modes were observed: E_2^H, expected at 568 cm^{-1}, and $A_1(LO)$, expected at 734 cm^{-1}, as indicated by the vertical dashed lines[23,24]. The sample grown at 60 W RF power has shown better-defined peaks, followed by the samples grown at 75 and 90 W. The samples grown at 45 and 30 W did not show clear phonon

modes peaks, which could be attributed, in part, to their low thicknesses (~200 and 100 nm, respectively), but can also indicate that those samples have lower crystalline quality, which will be explored forward regarding the XRD results.

In Figure 5, representative AFM and SEM images of the GaN films grown at 30, 60 and 90 W are shown. The SEM micrographs exhibited uniform, homogeneous and flat surfaces. In contrast with the GaN/Si films[16], neither clusters at 30W, nor elongated structures at 90 W were found, suggesting a possible influence of the glass substrate in the film formation. The total height variation in the AFM images of 2 µm x 2 µm scanning area were in range 30-42 nm, corroborating the flatness observed in the SEM images. The AFM micrographs also revealed surfaces formed by densely packed round nanoparticles (NPs), approximately 32 nm wide. The film surface topography can be quantitatively characterized by the R_{ms} roughness parameter, which is the root mean square of the heights and depths measured from a mean line ($z = 0$) and can be interpreted as the standard deviation of the surface profile from this mean line. The obtained R_{ms} values were 2.76 ± 0.08 nm, 7.78 ± 2.12 nm and 7.47 ± 1.03 nm, respectively for 30, 60 and 90 W. Compared with the samples at 60 and 90 W, the low dispersion for the film at 30 W reflects the better packing of the smaller NPs.
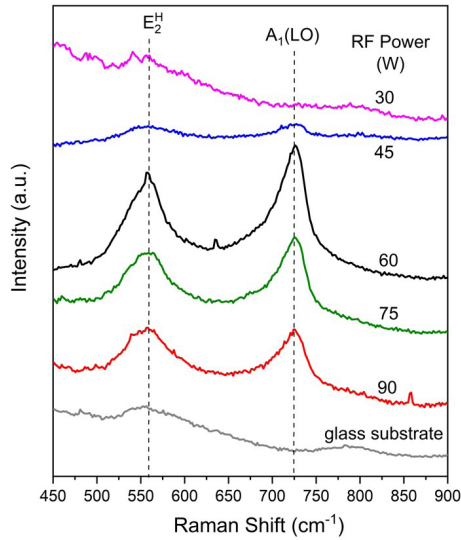
Figure 6 presents the cross-sectional SEM image of the GaN/glass film grown at 90 W (the thicker film of the series). The direct image-measured thickness of 736 nm confirms the values obtained by profilometry and by the transmittance spectrum. The image also exposes the dominant and dense columnar-like morphological structure of the film. Additionally, smaller nanostructures adjacent to the film/substrate interface were also observed. However, there is no distinct demarcation between these two morphologies. A very similar morphology was already reported in the literature[25] for GaN films grown onto amorphous silica. Moreover, this morphology is commonly observed on sputtered materials at relatively low substrate temperatures[26].

Figure 4. Raman spectra from the GaN/glass films grown at different RF powers. E_2^H and A_1(LO) phonon modes expected peak positions[23] are shown by dashed vertical lines.
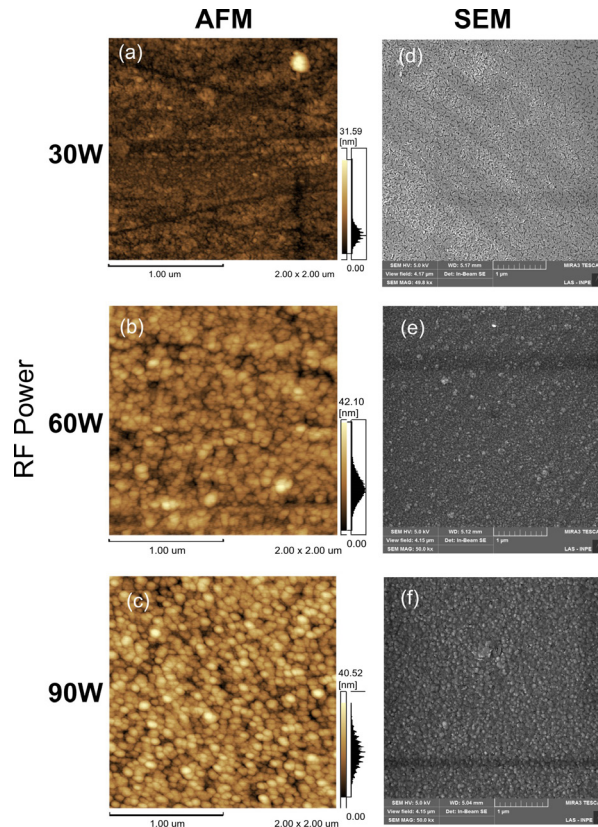
Figure 5. AFM and SEM micrographs of GaN/glass films grown with RF power of (a, d) 30 W, (b, e) 60 W and (c, f) 90 W, respectively.
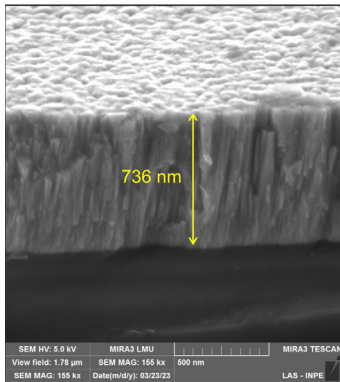
Figure 6. Cross-sectional SEM image of the GaN/glass film grown using RF power of 90 W.

Figure 7a shows X-ray diffractograms for each sample grown with different RF power applied to the Ga target, together with the respective thicknesses value as measured by profilometer. Only GaN wurtzite phase peaks were seen, and all the diffractograms have exhibited a pronounced (0002) diffraction peak indicating the preferential *c*-axis orientation of the crystallites[28]. Figure 7b highlights the region where the main GaN diffraction peaks ((10$\bar{1}$0), (0002), and (10$\bar{1}$1)) are observed. The crescent behavior of the (0002) peak intensities seen from 30 W to 90 W could be strictly related to the greater volume of crystallized material as the film becomes thicker. The maximum position of the (0002) peak has also noticeably changed with the RF power.

A more careful analysis revealed that the (0002) peak has two components, whose intensities are also RF power dependent. As shown in Figure 8, for 75 W, the (0002) diffraction peak is composed by a broad component at lower angle, here named as (0002)^a, and a sharp component at higher angle, named as (0002)^b. For the 30 W sample, the (0002) diffraction peak was satisfactorily described by only one-component. The central position of each deconvoluted XRD peak is presented in Figure 9, together with the respective reference values represented by dashed horizontal lines. Notice that the individual peak positions do not change significantly with respect to the RF power applied to the Ga target during the growth. Also, the (0002)^b peak position is very close to the expected value of (0002) wurtzite GaN diffraction peak position[27], while the other peaks, (10$\bar{1}$0), (0002)^a and (10$\bar{1}$1) have shown a significant shift to lower angles when compared to the respective expected values.

The full width at half maximum (FWHM) of the individual deconvoluted diffraction peaks was also plotted as a function of the RF power in Figure 10. It is possible to note that the (10$\bar{1}$0), (0002)^a and (10$\bar{1}$1) peaks have in common a relative larger FWHM values in the range of 0.4° - 0.8°, while the (0002)^b peak has narrow FWHM, less than 0.25°. The mean crystallite was estimated, using the Scherrer equation[29], from both (0002)^a and (0002)^b diffraction peaks, which is presented in Figure 3. The crystallite sizes obtained from (0002)^a are very small, and slowly decreased from 20 nm for 30 W to 10 nm for 90 W. Conversely, the estimated crystallite sizes estimated from the (0002)^b peak increase from approximately 70 nm for 45 W to the limit of the film thickness for 75 and 90 W.
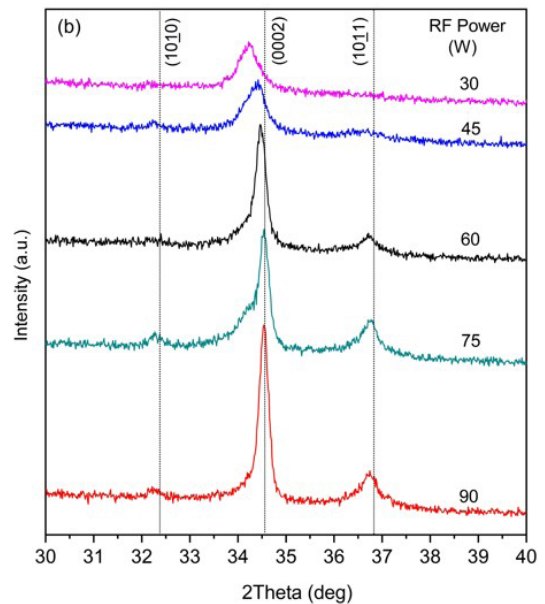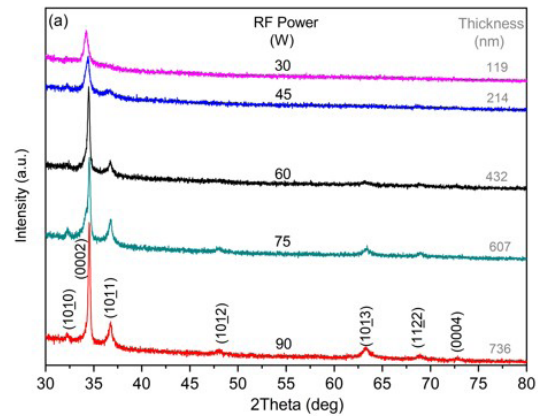
Figure 7. (a) X-ray diffractograms of the GaN/glass films grown using different RF power. (b) Expanded scale in the interval 30°-40°, showing the main diffraction peaks and respective expected peak positions (vertical dashed lines)[27].
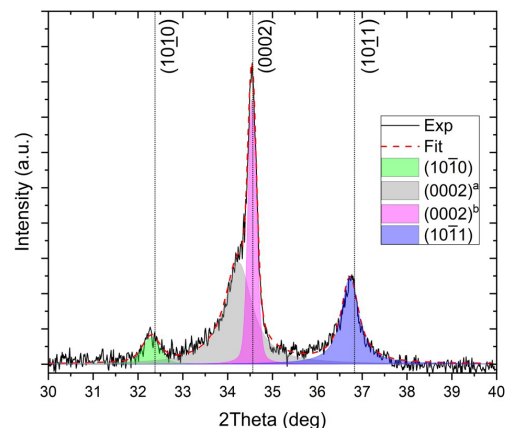
Figure 8. Deconvolution of the (0002) peak for the sample grown at 75 W using the HighScore® software. The vertical dashed lines show the expected peak positions[27].
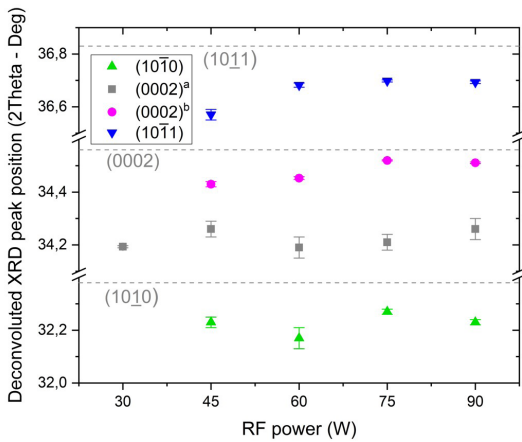
Figure 9. Deconvoluted diffraction peak position as a function of the RF power. The horizontal dashed lines represent the respective expected positions[27].
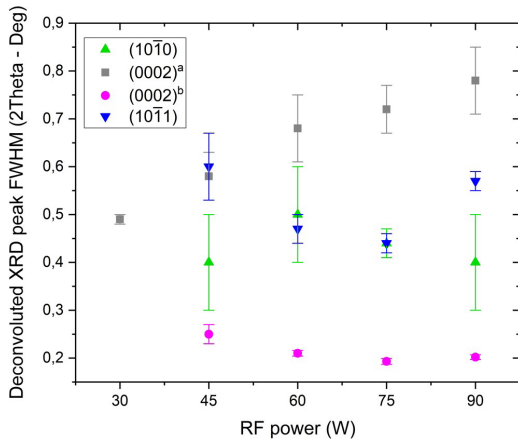
Figure 10. FWHM of each deconvoluted diffraction peak as a function of the RF power.

The XRD results thus indicate that the GaN/glass films grown with RF power from 45 to 90 W are composed by two different morphologies with the same wurtzite structure: one of small and tensioned crystallites with a weak preferential (0002), responsible for the broad and significantly dislocated $(10\bar{1}0)$, $(0002)^a$ and $(10\bar{1}1)$ diffraction peaks; and a second, of larger (thickness-size) crystallites strongly oriented in the <0002> direction, responsible for the sharp $(0002)^b$ diffraction peak. In addition to the SEM images, it can be concluded that the latter is in fact a columnar-like morphology composed of elongated crystallites arranged perpendicularly to the substrate, whose axis coincides with the wurtzite c-axis.

It is worth noting that the XRD (Figure 7b) from the films grown at lower RF powers (45 and 30 W) are dominated by the peaks attributed to the small crystallite morphology described above, and that the AFM and surface SEM images from the 30 W sample (Figure 5a,d) do not show clear formation of individual grains. These observations, in addition to the low thickness of these films, allow to conclude that the small crystallite morphology dominates the first nanometers of the growth, and thus could be forming an intermediate layer between the substrate and the columnar morphology for the thicker samples (60 to 90 W). This intermediate layer would then work as a self-buffer layer for the adjacent columnar morphology, relieving the tensions from the substrates and allowing a higher quality, highly oriented morphology with larger crystallites to take place. The formation of similar intermediate layer had already been intensively studied by TEM images in the GaN growth by sputtering onto amorphous silica[25] and it has been explained in terms of the van der Drift model[30]. Moreover, a model of the growth mechanism of this composition of morphologies was already proposed in the case of sputtered AlN films grown onto Si[31].

Although these two morphologies could be identified based on the XRD data in this present work for sputtered GaN/glass, the twin samples grown at the same deposition processes but onto crystalline Si (100) did not show the same aspect on the XRD results, or any evidence of formation of this double morphology, as shown on previous work[16]. Moreover, thicker GaN/Si samples (RF power above 60 W) showed less crystalline quality with poor c-axis preferred orientation. This conflict evidences the influence of the different substrates used, the amorphous glass substrates leading to the growth of a highly tensioned and self-limited layer with smaller grain size on the first tens of nanometers, which serves as buffer layer for the next morphology, which is then composed of more relaxed and larger crystallites. Meanwhile, the silicon substrates lead to a continuous growth of slightly tensioned films with morphology strongly dependent of the RF power applied to the Ga target[16].

4. Conclusions

This work reported on the main characteristics of GaN films grown onto glass substrates by reactive sputtering using different RF power applied to the substrates. The structural, morphological, vibrational, and optical properties of the samples were studied by XRD, AFM, SEM, Raman and UV-Vis transmittance. The films showed only wurtzite phase XRD peaks with dominant (0002) preferential orientation and strongly RF power-dependent thickness. From a careful XRD analysis, it was discriminated a self-limited intermediate layer composed of smaller and poorly oriented crystallites. This intermediate layer functioned as a buffer layer for the dominant film morphology of the thicker films, which is composed of larger and strongly c-axis oriented crystallites.

5. Acknowledgements

6. References

1. Leszczynski M, Teisseyre H, Suski T, Grzegory I, Bockowski M, Jun J, et al. Lattice parameters of gallium nitride. Appl Phys Lett. 1996;69(1):73-5. http://dx.doi.org/10.1063/1.118123.
2. Nakamura S. Current status of GaN-based solid-state lighting. MRS Bull. 2009;34:101-7. http://dx.doi.org/10.1557/mrs2009.28.

3. Greco G, Iucolano F, Roccaforte F. Review of technology for normally-off HEMTs with p-GaN gate. Mater Sci Semicond Process. 2018;78:96-106. http://dx.doi.org/10.1016/j.mssp.2017.09.027.

4. Müller A, Neculoiu D, Konstantinidis G, Deligeorgis G, Dinescu A, Stavrinidis A, et al. SAW devices manufactured on GaN/Si for frequencies beyond 5 GHz. IEEE Electron Device Lett. 2010;31(12):1398-400. http://dx.doi.org/10.1109/LED.2010.2078484.

5. Miškinis R, Jokubauskis D, Urba E, Smirnov D, Gaidamovičiūtė L, Mikalauskas K, et al. Investigation of a GaN-Based SAW oscillator with respect to UV illumination and temperature. Acta Phys Pol A. 2015;127:90-2. http://dx.doi.org/10.12693/APhysPolA.127.90.

6. Abdallah B, Jazmati AK, Refaai R. Oxygen effect on structural and optical properties of ZnO thin films deposited by RF magnetron sputtering. Mater Res. 2017;20(3):607-12. http://dx.doi.org/10.1590/1980-5373-MR-2016-0478.

7. Jazmati AK, Abdallah B. Optical and structural study of ZnO thin films deposited by RF magnetron sputtering at different thicknesses: a comparison with single crystal. Mater Res. 2018;21(3):1-6. http://dx.doi.org/10.1590/1980-5373-MR-2017-0821.

8. Schiaber ZS, Leite DMG, Bortoleto JRR, Lisboa-Filho PN, da Silva JHD. Effects of substrate temperature, substrate orientation, and energetic atomic collisions on the structure of GaN films grown by reactive sputtering. J Appl Phys. 2013;114(18):183515. http://dx.doi.org/10.1063/1.4828873.

9. Mulyo AL, Konno Y, Nilsen JS, van Helvoort ATJ, Fimland B-O, Weman H, et al. Growth study of self-assembled GaN nanocolumns on silica glass by plasma assisted molecular beam epitaxy. J Cryst Growth. 2017;480:67-73. http://dx.doi.org/10.1016/j.jcrysgro.2017.10.009.

10. Watanabe T, Ohta J, Kondo T, Ohashi M, Ueno K, Kobayashi A, et al. AlGaN/GaN heterostructure prepared on a Si (110) substrate via pulsed sputtering. Appl Phys Lett. 2014;104(18):182111. http://dx.doi.org/10.1063/1.4876449.

11. Junaid M, Hsiao CL, Chen YT, Lu J, Palisaitis J, Persson POÅ, et al. Effects of N2 Partial pressure on growth, structure, and optical properties of GaN nanorods deposited by liquid-target reactive magnetron sputter epitaxy. Nanomaterials (Basel). 2018;8(4):223. http://dx.doi.org/10.3390/nano8040223.

12. Müller A, Konstantinidis G, Giangu I, Adam GC, Stefanescu A, Stavrinidis A, et al. GaN Membrane supported saw pressure sensors with embedded temperature sensing capability. IEEE Sens J. 2017;17(22):7383-93. http://dx.doi.org/10.1109/JSEN.2017.2757770.

13. Dow ABA, Kherani NP, Popov C, Ahmed A, Schmid U. Nanocrystalline diamond/AlN structures for high efficient SAW nano-resonators. In: ISAF-ECAPD-PFM 2012; 2012; Aveiro, Portugal. Proceedings. USA: IEEE; 2012. p. 1-4. http://dx.doi.org/10.1109/ISAF.2012.6297775.

14. Lee S-H, Jeong H-H, Bae S-B, Choi H-C, Lee J-H, Lee Y-H. Epitaxially grown GaN thin-film SAW filter with high velocity and low insertion loss. IEEE Trans Electron Dev. 2001;48(3):524-9. http://dx.doi.org/10.1109/16.906446.

15. Izyumskaya N, Avrutin V, Ding K, Özgür Ü, Morkoç H, Fujioka H. Emergence of high quality sputtered III-nitride semiconductors and devices. Semicond Sci Technol. 2019;34(9):093003. http://dx.doi.org/10.1088/1361-6641/ab3374.

16. De Oliveira RS, Folli HA, Stegemann C, Horta IM, Damasceno BS, Miyakawa W, et al. Structural, morphological, vibrational and optical properties of gan films grown by reactive sputtering: the effect of rf power at low working pressure limit. Mater Res. 2022;25:e20210432. http://dx.doi.org/10.1590/1980-5373-MR-2021-0432.

17. Klein JD, Yen A, Cogan SF. Determining thin film properties by fitting optical transmittance. J Appl Phys. 1990;68(4):1825-30. http://dx.doi.org/10.1063/1.346617.

18. Cabrera CI, Contreras-Solorio DA, Hernández L. Joint density of states in low dimensional semiconductors. Physica E. 2016;76:103-8. http://dx.doi.org/10.1016/j.physe.2015.10.013.

19. O'Leary SK. An analytical density of states and joint density of states analysis of amorphous semiconductors. J Appl Phys. 2004;96(7):3680-6. http://dx.doi.org/10.1063/1.1778478.

20. Wemple SH, DiDomenico M. Optical dispersion and the structure of solids. Phys Rev Lett. 1969;23:1156-60. http://dx.doi.org/10.1103/PhysRevLett.23.1156.

21. Leite DMG, da Silva JHD. The optical absorption edge of nanocrystalline Ga1-xMnxN films deposited by reactive sputtering. J Phys Condens Matter. 2008;20(5):55001. http://dx.doi.org/10.1088/0953-8984/20/05/055001.

22. Muth JF, Brown JD, Johnson MAL, Yu Z, Kolbas RM, Cook JW, et al. Absorption Coefficient and Refractive Index of GaN, AlN and AlGaN alloys. MRS Internet J Nitride Semicond Res. 1999;4(Suppl 1):502-7. https://doi.org/10.1557/S1092578300002957.

23. Harima H. Properties of GaN and related compounds studied by means of Raman scattering. J Phys Condens Matter. 2002;14(38):R967-93. http://dx.doi.org/10.1088/0953-8984/14/38/201.

24. Chuah LS, Hassan Z, Abu Hassan H. Optical characterization of GaN thin film grown on Si(111) by radio-frequency plasma-assisted molecular beam epitaxy. In: Malaysia-Japan International Symposium on Advanced Technology 2007 (MJISAT 2007); 2007 Nov 12-15; Kuala Lumpur. Proceedings. Kuala Lumpur: Seri Pacific Hotel; 2007.

25. Leite DMG, Li T, Devillers T, Schiaber ZS, Lisboa-Filho PN, Bonanni A, et al. Columnar microstructure of nanocrystalline Ga1−xMnxN films deposited by reactive sputtering. J Cryst Growth. 2011;327(1):209-14. http://dx.doi.org/10.1016/j.jcrysgro.2011.05.012.

26. Kusano E. Structure-zone modeling of sputter-deposited thin films: a brief review. Applied Science and Convergence Technology. 2019;28:179-85. http://dx.doi.org/10.5757/ASCT.2019.28.6.179.

27. Heinz Schulz KH. Thiemann, crystal structure refinement of AlN and GaN. Solid State Commun. 1977;23(11):815-9. http://dx.doi.org/10.1016/0038-1098(77)90959-0.

28. Yadav BS, Major SS, Srinivasa RS. Growth and structure of sputtered gallium nitride films. J Appl Phys. 2007;102(7):073516. http://dx.doi.org/10.1063/1.2786100.

29. Birkholz M. Thin film analysis by X-ray scattering. Weinheim: Wiley-VCH; 2005. https://doi.org/10.1002/3527607595.fmatter.

30. Van der Drift A. Evolutionary selection, a principle governing growth orientation in vapour-deposited layers. Philips Res Rep. 1967;22(3):267.

31. Hwang BH, Chen CS, Lu HY, Hsu TC. Growth mechanism of reactively sputtered aluminum nitride thin films. Mater Sci Eng A. 2002;325(1-2):380-8. http://dx.doi.org/10.1016/S0921-5093(01)01477-0.